Supporting Information (SI) Appendix

Heterogeneous Binding of the SH3 Client Protein to the DnaK Molecular Chaperone

Jung Ho Lee[a,b], Dongyu Zhang[a,c], Christopher P. Hughes[a], Yusuke Okuno[a], Ashok Sekhar[a,d] and Silvia Cavagnero[a]

[a]Department of Chemistry, University of Wisconsin - Madison, 1101 University Ave., Madison, Wisconsin, 53706, USA. [b]Present address: Laboratory of Chemical Physics, National Institute of Diabetes and Digestive and Kidney Diseases, National Institutes of Health, 9000 Rockville Pike, Bethesda, MD, 20892, USA. [c]Present address: Department of Chemistry, Columbia University, MC 3178, 3000 Broadway, New York, NY, 10027, USA. [d]Present address: Departments of Molecular Genetics, Biochemistry and Chemistry, The University of Toronto, 1 King's College Circle, Toronto, Ontario, Canada, M5S 1A8.

Correspondence should be addressed to S.C. (Email: cavagnero@chem.wisc.edu, Phone: 608-262-5430).

SUPPLEMENTARY CALCULATIONS AND THEORETICAL CONSIDERATIONS

Estimate of molecular weight of substrate-free DnaK from DOSY NMR. To test whether the DOSY measurements yielded data consistent with a realistic molecular size for client-protein-free DnaK, the effective DnaK radius (r) was estimated from the experimental translational diffusion coefficient D_t of DnaK determined by 1D ^{1}H DOSY and the Stokes-Einstein relation

$$D_t = \frac{k_B T}{6\pi\eta r}, \quad (1)$$

where k_B is the Boltzmann constant, T is the temperature (set to 298K), and η is the solution viscosity. The above estimate assumes spherical shape. We then calculated the expected DnaK molecular weight MW (1) from

$$MW = V\frac{N}{(\bar{v}_p + \Delta\bar{v}_h)}, \quad (2)$$

where N is Avogadro's number, V is the volume of the macromolecule deduced from r, which was obtained upon entering D_t measured by DOSY into equation (1) and solving for r. The symbols $\bar{v}_p$ and $\bar{v}_h$ denote the partial specific volume of the macromolecule of interest and water (in $cm^3\,g^{-1}$), respectively, and Δ denotes the grams of bound water per gram of protein.

The above calculation led to the conclusion that, as expected, the MW of DnaK (and also that of the DnaK-SH3 complex, which is assumed to have similar size to substrate-free DnaK) is much larger than that of free SH3. It is worth noticing that the numerical value of the estimated MW obtained via this calculation is even larger than the actual molecular weight of the chaperone. This discrepancy is likely due to the fact that the above back-of-the-envelope calculation does not take into account the fact that ADP-DnaK is not exactly spherical (2).

Estimation of ^{15}N NMR linewidths of chaperone-free SH3 and the SH3-DnaK complex. *Prediction of theoretical linewidths.* An estimate of the expected ^{15}N linewidths of unfolded and native SH3, and of SH3-DnaK complexes was carried out starting from the apparent rotational

correlation times obtained from DOSY experiments. The rotational correlation time for the global macrmolecular motions (τ_c) was derived from the Stokes-Einstein-Debye equation assuming, for simplicity, a rigid body and spherical shape

$$\tau_c = \frac{\eta V}{k_B T} = \frac{4\pi\eta r^3}{3k_B T} \quad , \tag{3}$$

using the molecular radius of the hydrated macromolecule assessed as described in the previous section. The spectral density function J(ω) was then calculated according to the following simplified model-free expression (3-5), applicable to proteins in aqueous solution characterized by local and global dynamics, with local motions much faster than the global motions (6)

$$J(\omega) = \frac{S^2\tau_c}{1+(\tau_c\omega)^2}, \tag{4}$$

where ω is the frequency of interest and S is the order parameter. In the absence of detailed information on NH bond vector local dynamics gathered under the exact conditions of our experimental system, an approximate estimate was obtained under the limiting conditions of a rigid body upon setting the square of the order parameter to S^2=1.The expected transverse relaxation time, T_2, was then calculated from equations (5) – (7) according to reference (6)

$$\frac{1}{T_2} = 0.5d^2\{4J(0) + J(\omega_N - \omega_H) + 3J(\omega_N) + 6J(\omega_H) + 6J(\omega_N + \omega_H)\} + c^2\{3J(\omega_N) + 4J(0)\}, \tag{5}$$

with

$$d^2 = 0.1\gamma_H^2\gamma_N^2\hbar^2 < \frac{1}{r_{NH}^3} >^2, \tag{6}$$

and

$$c^2 = \left(\frac{2}{15}\right)\gamma_N^2 B_0^2(\sigma_\parallel - \sigma_\perp), \tag{7}$$

where $\omega_N$and ω_H are the ^{15}N and ^{1}H Larmor frequencies, respectively, γ_N and γ_H are the gyromagnetic ratios of ^{15}N and ^{1}H, respectively, r_{NH} is the bond length of the amide nitrogen-proton bond, $\sigma_\parallel \text{and} \sigma_\perp$ are the parallel and perpendicular components of the axially symmetric ^{15}N chemical shift tensor, and B_0 is the external magnetic field (an NH bond length of 1.02Å, and

$\sigma_{\parallel} - \sigma_{\perp}$ =-160ppm were used (6)). ^{15}N linewidths at half-height in Hz ($\Delta\upsilon$) were then estimated from

$$\Delta\upsilon = \frac{1}{\pi T_2} \quad . \tag{8}$$

Note that the above linewidth calculations include only ^{15}N dipolar relaxation from amide protons and chemical shift anisotropy. Other relaxation mechanisms (e.g., dipolar relaxation due to ^{13}C) are neglected. The resulting estimated linewidths are shown in Supplementary Table 1.

Note that the assumption of rigid spherical shape is likely not valid for the unfolded state, and may not be rigorously valid for the native state either. Transverse relaxation effects due to instrumental contributions (often referred to as $1/T_2$*) are also not taken into account. Hence the calculated values reported in Supplementary Table 1 should be regarded as approximate estimates of linewidth upper-limit values (neglecting instrumental contributions).

Comparison with experimental linewidths. Volume analysis (Fig. 6 of main article) shows that in the presence of DnaK the population of free unfolded SH3 is 6% of the total, and the population of spectroscopically detectable bound SH3 in equilibrium with the unfolded state is 24% of the total.

Let's consider the case of SH3 residues in fast-exchange on the transverse relaxation rate (R_2) timescale and hypothesize tumbling at the same rate as DnaK (i.e. rigidly bound). Under these conditions, the theoretical linewidth of these residues is a weighted average of the linewidths of the free and bound species (see Supplementary Table 1), according to:

$$\Delta\upsilon_{obs} = f_F\Delta\upsilon_F + f_B\Delta\upsilon_B \tag{9}$$

where $\Delta\upsilon_{obs}$ is the observed linewidth, $\Delta\upsilon_F$ and $\Delta\upsilon_B$ are the linewidths of the free and bound states, respectively, and f_F and f_B are the fractions of the free and bound species, respectively. The resulting estimated linewidth is ca. 32 Hz. This value represents a greater than 10-fold increase in ^{15}N linewidth compared to what is expected for SH3 alone. In case the proton linewidths were to broaden by a similar degree as those of ^{15}N estimated above, it is expected

that the 2D ^{1}H-^{15}N HSQC NMR resonance intensities of the DnaK-SH3 complex, whether in slow or fast exchange on the NMR chemical shift timescale, would decrease by more than 100-fold relative to SH3 alone, according to the simple arguments highlighted in the Appendix. The signal for these resonances would therefore be undetectable.

Thus, we conclude that the detectable resonances in fast exchange on the NMR chemical shift timescale cannot be due to a rigidly bound ligand, and must arise from residues which retain some local dynamics upon DnaK binding.

As described in the main manuscript, several new SH3 resonances in slow exchange on the NMR chemical shift timescale appear, upon addition of excess DnaK. The linewidth of these new resonances (Supplementary Fig. 4c), which are due to the bound state of SH3, is quite significant but not nearly close to the expected values for a rigidly chaperone-bound body. This experimental result confirms the prediction that the spectroscopically detectable bound resonances reflect the presence of bound SH3 that retains a residual degree of internal dynamics.

The volume analysis also revealed the existence of an additional significant population of SH3 (ca. 43%) formally invisible in the NMR spectrum. The above arguments predict that this particular population must be more rigidly bound to DnaK and is spectroscopically undetectable either due to relaxation losses during the NMR pulse sequence and(or) due to slow tumbling during the NMR acquisition time.

Viscosity-dependence of NMR linewidths. Rotational motions depend on the viscosity of the medium (Eq. 3). In order to evaluate the expected NMR linebroadening due solely to changes in viscosity (no binding events), we predicted the hypothetical rotational correlation time of SH3 in buffer in the presence of SH3 (given the experimentally determined viscosity= 0.98cP), and in the presence of DnaK (given the experimentally determined viscosity in the presence of DnaK =1.52cP), respectively. Then we computed the corresponding hypothetical ^{15}N linewidths from

Equations (3)-(8), assuming that the observed linebroadening was solely due to dipolar relaxation and chemical shift anisotropy.

From the apparent radius of unfolded and native SH3 in the absence of chaperone (obtained from DOSY and equation (1)), the hypothetical linewidths-at-half-height of unfolded and native SH3 in buffer alone were deduced to be 3.1 and 1.9 Hz, respectively.

In case only solution viscosity contributed to the line broadening of SH3 resonances in the presence of DnaK, the hypothetical linewidths would be 4.6 and 2.6Hz for the unfolded and native states, respectively (Supplementary Table 2). Hence, one can estimate the expected percent change in SH3 linewidths upon addition of DnaK assuming no binding were to take place according to

$$\%\,\Delta \mathrm{LW}_{\mathrm{hyp.}} = \frac{\left(\mathrm{LW}_{@1.52\ \mathrm{cp}} - \mathrm{LW}_{\ @0.98\ \mathrm{cp}}\right)}{\mathrm{LW}_{@0.98\ \mathrm{cp}}} \times 100\% \quad , \tag{10}$$

where% ΔLW_{hyp} is the expected percent increase in ^{15}N SH3 linewidths due solely to viscosity changes, and $LW_{@1.52cp}$ and $LW_{@0.98cp}$ are the hypothetical ^{15}N SH3 linewidths at the experimentally determined 1.52cP and 0.98cP viscosities of buffer alone and buffer in the presence of DnaK, respectively.

Entering appropriate numerical values into relation (10) for native and unfolded SH3 yields

$$\%\,\Delta \mathrm{LW}_{\mathrm{hyp.N}} = \frac{(2.6\ \mathrm{Hz} - 1.9\ \mathrm{Hz})}{1.87\ \mathrm{Hz}} \times 100\% = 37\% \tag{11}$$

and

$$\%\,\Delta \mathrm{LW}_{\mathrm{hyp.U}} = \frac{(4.6\ \mathrm{Hz} - 3.1\ \mathrm{Hz})}{3.1\ \mathrm{Hz}} \times 100\% = 48\% \quad , \tag{12}$$

where % $\Delta LW_{hyp,N}$, % $\Delta LW_{hyp,\,U}$ are the expected percent increases in ^{15}N linewidth for native and unfolded SH3, respectively, due solely to changes in viscosity upon addition of DnaK chaperone.

In summary, the expected percent of NMR linebroadening resulting merely from viscosity changes due to the addition of DnaK are estimated to be 37% and 48% for native and unfolded SH3, respectively.

Somewhat larger-than-expected linewidth increases are observed experimentally for the unfolded SH3 resonances that experience no chemical-shift changes in the presence of DnaK (Supplementary Fig. 4b). These resonances (except for the N terminus and residues 42-46) are due to the chaperone-free state in slow exchange on the chemical shift timescale. The broadening of these resonances beyond a mere viscosity contribution (>48% ^{15}N linewidth changes) is likely due to some degree of residual exchange broadening (7).

As mentioned in a previous section, the assumption of rigid spherical shape is likely not valid for the unfolded state, and may not rigorously apply to the native state either. Therefore the calculated values should be merely regarded as approximate estimates.

Finally, we also performed alternative estimates starting from experimentally determined values of rotational correlation times for global motions (τ_c) and order parameters (averaged over all residues) of chaperone-free native (N) and unfolded (U) states of SH3 published by Farrow and coworkers at different temperatures (8). We estimated variations in τ_c resulting from increased viscosity (due to addition of DnaK) from data reported under conditions leading to similar viscosity variations (8) as those that we experimentally observed. While estimated ^{15}N linewidths differed from the calculated values in Table 2, the expected percent increase in ^{15}N linewidths upon addition of chaperone was found to be 33% for the N state, and 42% for the U state. These values are very similar to those reported for N and U in our original calculations (see above) and graphically shown in Supplementary Figure S4 (horizontal dashed lines in panels a and b).

Additional comments on the Clean-SEA HSQC NMR experiments. The CLEANEX-PM pulse train that we employed is integrated within the CLEAN-SEA HSQC pulse sequence. The

CLEAN-SEA HSQC pulse sequence by Lin *et al.* (9) is advertised by the authors as artifact-free and it supposedly largely eliminates intra- and inter-molecular NOE contributions. Intra-molecular NOEs are eliminated by the CLEANEX-PM mixing/spin-lock period. Prior to that, the double $^{13}C/^{15}N$ filter eliminates all the magnetization resulting from protons covalently linked to ^{13}C or ^{15}N, in the SH3 $^{13}C/^{15}N$-doubly labeled protein. Hence we believe that the latter filter should also help decreasing inter-molecular NOEs from (unlabeled) DnaK to (doubly-labeled) SH3, though this effect may not be quantitative. In our experiments, we focused on the decrease in the observed CLEAN-SEA HSQC volumes (relative to SE HSQC), to qualitatively identify overall exchange-protected regions. In case some inter-molecular-NOEs were still present in our samples, these would lead to an attenuation of the observed exchange protection. The fact that we do observe a significant extent of exchange protection in the central region of the SH3 sequence gives us confidence that this effect is genuine.

Regarding conformational exchange, in the CLEAN-SEA HSQC pulse sequence, the 100 ms CLEANEX-PM pulse train corresponds to the mixing time when the fast-exchanging amide protons have the opportunity to build up magnetization. During this time, in addition to proton exchange at the amide sites, conformational exchange also takes place. The CLEAN-SEA HSQC data shown in Figure 7 report on the convoluted proton exchange behavior of all the amide protons that exchange fast on the 100 ms timescale. In this sense, it is fair to state that the CLEAN-SEA HSQC experiment is somewhat qualitative, and is unable to discriminate the individual behavior of all the different conformational states.

MATERIALS AND METHODS

Protein expression and purification. Unlabeled and isotopically labeled SH3 was expressed and purified as described (10, 11). Purified ^{1}H, ^{13}C-enriched SH3 was characterized by electrospray mass spectrometry [average MW_{theor}= 6,859.6 (unlabeled), 7,231.3 (labeled at 99% level); average MW_{exper}= 7,226.3 (labeled at nominal 99% level)]. Stock solutions of pure SH3

were stored in 50 mM Tris (pH 7.2), 5 mM $MgCl_2$, and 50 mM KCl, flash-frozen and stored at -80°C. DnaK was prepared either according to published procedures (12) or according to the following streamlined procedure. The wild type DnaK gene was subject to PCR amplification and subcloned into the linearized Champion™ pET SUMO vector (Invitrogen, Carlsbad, CA). The plasmid was then transformed into BL21-CodonPlus (DE3)-RIPL (Agilent Technologies, Palo Alto, CA) competent cells and grown in LB media with 50 μg/mL kanamycin at 37 °C. Protein overexpression was induced by addition of IPTG at OD600 of 0.7-0.8. After induction, the cells were harvested after 24 hrs of incubation under shaking (250 r.p.m.) at 25 °C. The cells were resuspended and sonicated in a buffer containing 30 mM potassium phosphate (pH 7.4), 500 mM KCl, 30 mM imidazole, and 2 mM PMSF. The cell lysate was centrifuged for 30 min at 15,000 rpm (SS-34 rotor, Thermo Scientific, Waltham, MA) and the supernatant was applied to the HisTrap HP column (GE Healthcare, Piscataway, NJ) and eluted with a buffer containing 30 mM sodium phosphate (pH 7.4), 500 mM KCl, and 500 mM imidazole. After dialysis of the eluted fractions against 50 mM Tris-HCl (pH 7.4), 150 mM KCl, 1 mm DTT, and 30 mM imidazole buffer, 10,000 units of His-tagged SUMO protease (SP-400, MCLAB, South San Francisco, CA) per liter of cell culture were added and incubated for 9 hrs at room temperature. This procedure led to more than 50% cleavage of His-SUMO-DnaK as assessed by SDS-PAGE. After spinning down the reaction mixture to remove any insoluble aggregates, the supernatant was loaded on the HisTrap HP column again and the flow through was collected and verified to have only wild-type DnaK and no His-SUMO-DnaK, His-SUMO tag or His-tagged SUMO protease, by SDS-PAGE. Note that the SUMO protease was His-tagged. Finally, size exclusion chromatography was performed on a Superdex 200 column (GE Healthcare, Piscataway, NJ) using 30 mM potassium phosphate (pH 7.4) in the presence of 500 mM KCl as elution buffer. Wild-type DnaK-containing fractions were collected, concentrated and dialyzed against the NMR buffer (50 mM Tris, 5 mM $MgCl_2$, 50 mM KCl, pH 7.2).

NMR sample preparation. In the case of NMR samples containing only ^{13}C-^{15}N-SH3, a solution of the pure protein in storage buffer was diluted to a final concentration of 300 μM in 50 mM Tris (pH 7.2), 5 mM $MgCl_2$, 50 mM KCl, 5 mM ADP and 15 mM DTT in 5% v/v D_2O. SH3 samples containing ADP-DnaK were prepared identically except for the presence of 1.2 mM of DnaK. The latter sample becomes slightly cloudy presumably due to the release and aggregation of previously bound DnaK substrates, released upon the binding of DnaK and SH3. The cloudiness disappeared after 24 hours of incubation at room temperature and ultracentrifugation at 115,000 r.p.m. (TLA-120.1 rotor, Beckman Coulter, Fullerton, CA). The supernatant was collected for NMR experiments.

NMR data collection and analysis. Unless otherwise noted, all NMR experiments were performed using an Agilent 600 MHz (14.1 T) NMR spectrometer equipped with a 5 mm z-axis PFG triple resonance cryogenically cooled probe. All NMR experiments were carried out at 25°C. All data were processed with NMRPipe (13) (Version 9.0.0-b108) and analyzed with NMRviewJ (14) (Version 2009.015.15.35). Volume measurements were carried out using the AutoFit script of NMRPipe.

^{1}H-^{15}N SE HSQC. We employed a sensitivity-enhanced pulse field gradient ^{1}H-^{15}N HSQC sequence (7, 15).

Sweep widths were set to 10,000 Hz and 1937 Hz with 512 and 256 complex data points, in the direct and indirect dimensions, respectively. 18°- and 27°-shifted cosine-bell-square apodization was applied to the direct and indirect dimensions, respectively.

SH3 backbone assignments. Backbone assignments for both folded and unfolded ^{13}C,^{15}N-labeled SH3 were performed with the HNCACB (16), CBCA(CO)NH (17), HNCO (18) and (HCA)CO(CA)NH (19) pulse sequences (BMRB accession number 25501). Parameters for these experiments are provided in Supplementary Table 3. Heteronuclear exchange spectroscopy (20, 21) was employed to verify some of the assignments. All experiments leading to backbone assignments were performed at pH 7.2 and 25°C in NMR buffer. Assignments

were consistent with previous assignments under different buffer conditions (22). Tryptophan indole resonances were assigned by analogy to previously published data (23). Backbone assignments of SH3 resonances in the presence of a 4-fold excess of ADP-DnaK were carried out under similar experimental conditions and by similar experiments to those listed above (BMRB accession number 25500). The triple-resonance experiments in the presence of DnaK also included the acquisition of an HNCA data set.

Diffusion ordered spectroscopy. The translational diffusion of SH3 (0.3 mM) in the absence and presence of ADP-DnaK (1.2 mM) was measured by diffusion ordered NMR spectroscopy (DOSY NMR). The convection-compensated (24) one-shot (25) 2D DOSY pulse sequence was integrated within sensitivity-enhanced ^{1}H-^{13}C SE HSQC (26) to probe the diffusion of SH3 alanine methyl groups, whose assignments were confirmed by HBHA(CO)NH (27). The ^{1}H and ^{13}C sweep widths were 10,000 and 2,000 Hz, with 1024 and 32 complex data points in the direct and indirect dimensions, respectively. Unshifted cosine-bell square apodization was applied in both dimensions. The translational diffusion of unlabeled ADP-DnaK (0.3 mM) was probed by an experiment employing the DOSY pulse train followed by a ^{1}H acquisition sequence employing the WATERGATE pulse train for solvent suppression (28). The diffusion coefficients were calibrated by setting the gradient powers so that the experimentally observed HDO diffusion coefficient at 25°C became equal to the known value of 19.02×10^{-10} m^2 s^{-1} (29) . Data for translational diffusion experiments were collected once, except for the samples containing both SH3 and DnaK, which displayed some low-intensity resonances. For these samples, the results of three independent experiments were averaged. The intense side-chain Ala_{13} methyl group was monitored for the DOSY analysis. The Ala_5 and Ala_{11} side-chain methyl groups were also analyzed for the unfolded state, and similar results were obtained. The DOSY decay curves and processed data are shown in Supplementary Figure S9.

Viscosity corrections of diffusion data. Translational diffusion coefficients were corrected for differences in viscosity due to variable protein concentrations in each sample, according to

known procedures (30). Briefly, we corrected all experimentally determined diffusion coefficients to simulate a scenario according to which all samples have the viscosity of the plain NMR buffer. According to the Stokes-Einstein equation, the translational diffusion coefficient is

$$D_t = \frac{k_B T}{6\pi\eta r} \quad , \qquad (1)$$

where k_B is the Boltzmann constant, T is temperature and η is the viscosity. Relation (1) can be applied to the hypothetical diffusion coefficient at the viscosity of the buffer ($D_{t,corr}$) and then divided by the corresponding equation at the observed sample viscosity ($D_{t,obs}$) to yield

$$D_{t,\,corr} = \frac{D_{t,obs}\eta_{obs}}{\eta_{buff}} \quad . \qquad (2)$$

Relation (2) enables correcting all experimental diffusion coefficients for variations in sample viscosity. The above corrected values were used to compute the fractions of chaperone- free and bound unfolded SH3. Corrected translational diffusion coefficients were regarded as the weighted average of diffusion coefficients of the bound and the free forms, so that

$$D_{t,\,corr,} = f_{FU} D_{t,\,FU} + f_{BU} D_{t,BU}, \qquad (3)$$

and

$$f_{FU} + f_{BU} = 1, \qquad (4)$$

where f denotes the mole fraction of the total unfolded SH3 that is either free in solution (FU) or DnaK-bound (BU). Knowing $D_{t,corr,}$, $D_{t,FU}$, and $D_{t,BU}$, relations (3) and (4) can be solved to identify the fractions of the free and bound unfolded species. We independently determined the diffusion coefficient of native SH3, $D_{t,FU,}$ from a pure ^{13}C,^{15}N-SH3 sample, and the diffusion coefficient of DnaK, $D_{t,BU}$, from a pure unlabeled DnaK sample. Given that DnaK is much larger than SH3, we made the first-order approximation that $D_{t,DnaK} \sim D_{t,BU.}$ Viscosities of all samples were measured on a microVisc viscometer (Rheosense, San Ramon, CA) at 25 °C.

Clean-SEA-HSQC. Clean-SEA-HSQC (9) experiments, employing the CLEANEX-PM pulse train (31), were performed on an INOVA 600MHz (14.1 T) NMR spectrometer equipped with a triple resonance $^1H\{^{13}C, ^{15}N\}$ triple-axis gradient probe at 25 °C. Sample temperature, pH and

buffer were the same as for the other NMR experiments. We examined SH3 in the absence and presence of ADP-DnaK to study the extent of solvent exposure of the different SH3 backbone amides. Sample concentration and solution conditions were the same as those of the other NMR experiments. Spectral widths were 10,000Hz and 1,945 Hz for the direct and indirect dimensions, respectively. The spin-lock γB1 field was set to 5.3 kHz. The relaxation delay was set to 2.0 s. The mixing time was set to 100ms. The number of scans was set to 8 and 64 for SH3 in the absence and presence of DnaK, respectively. The number of scans for the SH3 sample in the presence of DnaK is higher due to low signal-to-noise. The number of increments in the indirect dimension was set to 256. Reference ^{1}H-^{15}N SE HSQC spectra (7, 15) were recorded with similar data collection parameters (256 increments in the indirect dimension, and 8 and 64 transients, in the absence and presence of DnaK, respectively). To elucidate the contribution of DnaK to hydrogen exchange of SH3 with solvent, HSQC-normalized volume changes were computed from

$$\Delta\text{Volume} = \left[\frac{V_{CLN,S+D}}{V_{HSQC,S+D}}\right] - \left[\frac{V_{CLN,S}}{V_{HSQC,S}}\right], \quad (5)$$

where $V_{CLN,S}$ and $V_{CLN,S+D}$ are the volume of each resonance in the Clean-SEA-HSQC of SH3 in the absence and presence of DnaK, respectively. $V_{HSQC,S}$ and $V_{HSQC,S+D}$ are the corresponding corrected volumes in the ^{1}H,^{15}N HSQC. Given that clean-SEA-HSQC data were collected with more transients than the ^{1}H,^{15}N HSQC data, the volumes obtained from the latter experiment were corrected as follows

$$V_{HSQC}=V_{HSQC,\,OBS}\frac{n_{CLN}}{n_{HSQC}} \quad , \quad (6)$$

where $V_{HSQC,OBS}$ is the observed volume of the resonance in the ^{1}H,^{15}N HSQC spectrum, and n_{CLN} and n_{HSQC} are the number of transients in the Clean-SEA-HSQC and ^{1}H,^{15}N HSQC spectra, respectively.

Native gel analysis and binding isotherms. Samples for native gel analysis were prepared identically to the NMR samples, except that the buffer was 40 mM Tris-HCl and contained 10%

v/v glycerol. All samples had a final concentration of 40 μM SH3 and variable DnaK concentrations (from 10 to 400 μM). Samples were incubated overnight at room temperature before loading them on the gel. Non-denaturing PAGE (32) was performed on a vertical gel electrophoresis apparatus (Bio-Rad, Hercules, CA) at constant voltage (200V) for 35 min at room temperature. The gel consisted of 375 mM Tris-HCl (pH 8.8), 7.7% w/v acrylamide and 0.3% w/v bis-acrylamide. The gel running buffer consisted of 25 mM Tris and 192 mM glycine. Coomassie blue was used for both gel tracking and staining. Native gel images were collected on a Typhoon FLA 9500 laser scanner (General Electric, Fairfield, CT) upon excitation at 635 nm (with a Fuji-Film LPR/R665 filter) and analyzed with the Carestream Molecular Imaging software (Bruker, Billerica, MA). Intensities of each SH3 band in the presence of DnaK (band 1, see Fig. 3c) for each lane were divided by the corresponding intensities in lanes containing pure SH3 at the same concentration. These normalized intensities are defined as the fraction of free SH3. From these values, fractions of bound SH3 (f_B) and concentrations of free DnaK ([D]) were determined. Plots of f_B as a function of [D] were fit to

$$f_B = [D] / ([D] + K_d). \quad (7)$$

The latter relation was derived assuming that the SH3-DnaK complex C dissociates into free SH3 (S) and free DnaK (D) according to $C \rightleftharpoons S + D$, with dissociation constant

$$K_d = \frac{[S]\,[D]}{[C]} \quad . \quad (8)$$

Solving for [C] yields

$$[C] = \frac{[S]\,[D]}{K_d} \quad . \quad (9)$$

The fraction of DnaK-bound SH3, f_B, is

$$f_B = \frac{[C]}{[S]+[C]} \quad . \quad (10)$$

Substitution of (9) into (10) yields relation (7).

Mass spectrometry analysis of native gel bands. *Enzymatic in-gel digestion.* In-gel digestion and mass spectrometry analysis were performed at a local Mass Spectrometry Facility (U. Wisconsin-Madison Biotechnology Center). Gel bands from pertinent regions of native gels were excised and fragmented into small parts. Coomassie R-250-stained gel pieces were de-stained completely in MeOH/ H_2O/NH_4HCO_3 [50%:50%:100mM], dehydrated for 2min in ACN/H_2O/NH_4HCO_3 [50%:50%:25mM] then once more for 30sec in 100% ACN, dried in a Speed-Vac for 1min., rehydrated with 20µl of trypsin solution with 0.01% ProteaseMAX surfactant [10ng/µl trypsin (Trypsin Gold from PROMEGA Corp.) in 25mM NH_4HCO_3/0.01% w/v of ProteaseMAX (Promega Corp.)], let stand for 2min at room temperature. Additional 30µl of overlay solution [25mM NH4HCO3/0.01% w/v of ProteaseMAX (Promega Corp.)] was added to keep gel pieces immersed throughout the digestion. The digestion was conducted for 3hrs at 42°C, peptides generated from digestion were transferred to a new Protein LoBind tube (~50µl volume) and digestion was terminated by acidification to a 0.3% final trifluoroacetic acid (TFA) concentration. Samples were spun for 10min at max speed in a tabletop centrifuge to pellet down degraded ProteaseMAX and the supernatant was transferred to a new Protein LoBind tube.

Enzymatic in-liquid digestion. drkN SH3 (9µg) was denatured upon addition of an 8M Urea / 50mM NH_4HCO_3 (pH8.5) / 1mM Tris HCl stock solution for 5 min, then diluted to 25µl for tryptic digestion with 1.25µl MeOH, 13µl 25mM NH_4HCO_3 (pH8.5) and 2µl of trypsin/Lyc-C solution (100ng/µl Trypsin/Lys-C Mix from PROMEGA Corp. in 25mM NH_4HCO_3). Digestion was conducted for 2 hrs at 42°C, then an additional 1µl of trypsin/Lyc-C solution was added and digestion let proceed overnight at 37°C. The process was quenched by acidification to a 0.3% final TFA concentration. The mixture was then diluted 1:1 with 0.1% formic acid and submitted to nanoLC-MS/MS analysis.

NanoLC-MS/MS. Peptides resulting from tryptic digestion were analyzed by nanoLC-MS/MS using the Agilent 1100 nanoflow system (Agilent, Palo Alto, CA) connected to a hybrid linear ion

trap-orbitrap mass spectrometer (LTQ-Orbitrap, Thermo Fisher Scientific, Bremen, Germany) equipped with an EASY-Spray™ electrospray source. Chromatography of peptides prior to mass spectral analysis was accomplished using C18 reverse phase HPLC trap column (Zorbax 300SB-C18, 5µM, 5x0.3mm, Agilent) and capillary emitter column (PepMap® C18, 3µM, 100Å, 150x0.075mm, Thermo Fisher Scientific) onto which extracted peptides were automatically loaded. NanoHPLC system delivered solvents A: 0.1% (v/v) formic acid in water, and B: 95% (v/v) acetonitrile, 0.1% (v/v) formic acid at 0.30 µL/min, to elute peptides directly into the nano-electrospray over a 20 minutes 0% (v/v) B to 40% (v/v) B followed by 5 minute 40% (v/v) B to 100% (v/v) B gradient. As peptides eluted from the HPLC-column/electrospray source survey MS scans were acquired in the Orbitrap spectrometer with a resolution of 100,000 and up to 5 most intense peptides per scan were fragmented and detected in the ion trap over the 300 to 2000 m/z; redundancy was limited by dynamic exclusion. Raw MS/MS data were converted to mgf file format using MSConvert (ProteoWizard: Open Source Software for Rapid Proteomics Tools Development). Resulting mgf files were used to search against user defined database consisting of target protein plus common contaminants (106 protein entries). Peptide mass tolerance was set at 20 ppm and fragment mass at 0.8 Da. Due to low number of protein entries for statistical determination of significance in peptide matches, all relevant hits were manually reviewed.

Computation of Electrostatic Surface Potential. PDB files were converted to PQR format with the PDB2PQR software (33, 34) and used as input for electrostatic surface potential calculations solving the nonlinear Poisson-Boltzmann equation with the Adaptive Poisson-Boltzmann Solver (APBS) software package (35). DnaK was treated as a dielectric continuum with dielectric constant 2.0 embedded in a solvent of dielectric constant 80.0. In Fig. 1c, the molecular surface is colored according to the electrostatic charge of the solvent-accessible surface area with a solvent radius of 1.4Å. Blue denotes regions of positive potential (>+1 k_BT/e) and red denotes regions of negative potential (<-1k_BT/e). k_BT is 4.11 X 10^{-21} J at room

temperature where k_B is the Boltzmann constant in J/Kelvin (K), T is the temperature in K, and e is the charge of a single electron in Coulomb. Electrostatic surface potentials were viewed with the PyMOL software package (PyMOL Molecular Graphics System, Version 1.3r1 Schrödinger, LLC) equipped with the APBS plug-in.

APPENDIX

Notes on linewidth dependence of 2D NMR resonance intensities. The 2D absorption lineshape of a ^{1}H-^{15}N heteronuclear correlation experiment can be described as (36)

$$S(\omega_N, \omega_H) = a_N a_H \quad , \tag{13}$$

where

$$a_N(\omega_N) = \frac{\lambda_N}{(\omega_N - \omega'_N)^2 + (\lambda_N)^2} \tag{14}$$

and

$$a_H(\omega_H) = \frac{\lambda_H}{(\omega_H - \omega'_H)^2 + (\lambda_H)^2} \quad , \tag{15}$$

where ω_N and ω_H are the variable frequencies along the lineshape of the resonance of interest, ω'_N and ω'_H are the Larmor frequencies of the resonance of interest, and λ_N and λ_H are the transverse relaxation rate constants, of the nitrogen and hydrogen nuclei, respectively, in radians/s, where $\lambda = 1/T_2$. At the resonance maximum, $\omega_H = \omega'_H$ and $\omega_N = \omega'_N$. Hence, according to relations (13)-(15), the intensity of the resonance of interest is

$$S(\omega'_N, \omega'_H) = \frac{1}{\lambda_N} * \frac{1}{\lambda_H} \tag{16}$$

In conclusion, the intensity of 2D resonances is expected to be inversely proportional to the product of the linewidths-at-half-height in each dimension.

Supplementary References

1. Cantor CR & Schimmel PR (1980) *Biophysical chemistry: Part II: Techniques for the study of biological structure and function* (W.H. Freeman and Company, New York, NY).
2. Swain JF*, et al.* (2007) Hsp70 chaperone ligands control domain association via an allosteric mechanism mediated by the interdomain linker. *Mol. Cell* 26(1):27-39.
3. Lipari G & Szabo A (1982) Model-free approach to the interpretation of nuclear magnetic resonance relaxation in macromolecules. 1. Theory and range of validity. *J. Am. Chem. Soc.* 104(17):4546-4559.
4. Lipari G & Szabo A (1982) Model-free approach to the interpretation of nuclear magnetic resonance relaxation in macromolecules. 2. Analysis of experimental results. *J. Am. Chem. Soc.* 104(17):4559-4570.
5. Abragam A (1961) *The principles of nuclear magnetism* (Clarendon Press, Oxford, UK).
6. Kay LE, Torchia DA, & Bax A (1989) Backbone dynamics of proteins as studied by ^{15}N inverse detected heteronuclear NMR spectroscopy: application to staphylococcal nuclease. *Biochemistry* 28(23):8972-8979.
7. Cavanagh J, Fairbrother, W.J., Palmer III, A.G., Skelton, N.J. (2007) *Protein NMR Spectroscopy: Principles and Practice* (Academic Press, San Diego).
8. Farrow NA, Zhang, O., Forman-Kay, J.D., Kay, L.E. (1997) Characterization of Backbone Dynamics of Folded and Denatured States of an SH3 Domain. *Biochemistry* 36:2390-2402.
9. Lin DH, Sze KH, Cui YF, & Zhu G (2002) Clean SEA-HSQC: A method to map solvent exposed amides in large non-deuterated proteins with gradient-enhanced HSQC. *J. Biomol. NMR* 23(4):317-322.
10. Bezsonova I, Singer A, Choy WY, Tollinger M, & Forman-Kay JD (2005) Structural comparison of the unstable drkN SH3 domain and a stable mutant. *Biochemistry* 44(47):15550-15560.

11. Lee JH, Sekhar A, & Cavagnero S (2011) ^{1}H-Detected ^{13}C Photo-CIDNP as a Sensitivity Enhancement Tool in Solution NMR. *J. Am. Chem. Soc.* 133(21):8062-8065.

12. Sekhar A, Santiago M, Lam HN, Lee JH, & Cavagnero S (2012) Transient interactions of a slow-folding protein with the Hsp70 chaperone machinery. *Protein Sci.* 21(7):1042-1055.

13. Delaglio F*, et al.* (1995) Nmrpipe - a Multidimensional Spectral Processing System Based on Unix Pipes. *J. Biomol. NMR* 6(3):277-293.

14. Johnson BA & Blevins RA (1994) NMRView - a Computer-Program for the Visualization and Analysis of Nmr Data. *J. Biomol. NMR* 4(5):603-614.

15. Kay LE, Keifer P, & Saarinen T (1992) Pure Absorption Gradient Enhanced Heteronuclear Single Quantum Correlation Spectroscopy with Improved Sensitivity. *J. Am. Chem. Soc.* 114(26):10663-10665.

16. Grzesiek S, Bax, A. (1992) Correlating backbone amide and side-chain resonances in larger proteins by multiple relayed triple resonance NMR. *J. Am. Chem. Soc.* 114:6291-6293.

17. Grzesiek S & Bax A (1992) An Efficient Experiment for Sequential Backbone Assignment of Medium-Sized Isotopically Enriched Proteins. *J. Magn. Reson.* 99(1):201-207.

18. Kay L, Ikura M, Tschudin R, & Bax A (1990) 3-Dimensional Triple Resonance NMR Spectroscopy of Isotopically Enriched Proteins. *J. Magn. Reson.* 89:496-514.

19. Lohr F & Rutejans H (1995) A New Triple Resonance Experiment for the Sequential Assignment of Backbone Resonances in Proteins. *J. Biomol. NMR* 6:189-197.

20. Montelione GT & Wagner G (1989) 2D Chemical-Exchange NMR-Spectroscopy by Proton-Detected Heteronuclear Correlation. *J. Am. Chem. Soc.* 111(8):3096-3098.

21. Farrow NA, Zhang OW, Forman-Kay JD, & Kay LE (1994) A Heteronuclear Correlation Experiment for Simultaneous Determination of ^{15}N Longitudinal Decay and Chemical-Exchange Rates of Systems in Slow Equilibrium. *J. Biomol. NMR* 4(5):727-734.

22. Zhang O, Kay LE, Olivier JP, & Forman-Kay JD (1994) Backbone 1H and 15N resonance assignments of the N-terminal SH3 domain of drk in folded and unfolded states using enhanced-sensitivity pulsed field gradient NMR techniques. *J. Biomol. NMR* 4(6):845-858.

23. Zhang OW, Kay LE, & Forman-Kay JD (1995) Structural Characterization of a Folded and an Unfolded State of an Sh3 Domain in Aqueous Buffer and Solution Structure of This Domain by NMR. *J. Cell. Biochem.*:53-53.

24. Jerschow A & Muller N (1997) Suppression of convection artifacts in stimulated-echo diffusion experiments. Double-stimulated-echo experiments. *J. Magn. Reson.* 125(2):372-375.

25. Pelta MD, Morris GA, Stchedroff MJ, & Hammond SJ (2002) A one-shot sequence for high-resolution diffusion-ordered spectroscopy. *Magn. Reson. Chem.* 40:S147-S152.

26. Rajagopalan S, Chow CK, Fry C, Ragunathan V, & Cavagnero S (2004) NMR spectroscopic filtration of polypeptides and proteins in complex mixtures. *J. Biomol. NMR* 29:505-516.

27. Grzesiek S & Bax A (1993) Amino-Acid Type Determination in the Sequential Assignment Procedure of Uniformly C-13/N-15-Enriched Proteins. *J. Biomol. NMR* 3(2):185-204.

28. Piotto M, Saudek V, & Sklenar V (1992) Gradient-Tailored Excitation for Single-Quantum NMR-Spectroscopy of Aqueous-Solutions. *J. Biomol. NMR* 2(6):661-665.

29. Longsworth L (1960) The Mutual Diffusion of Light and Heavy Water. *J. Phys. Chem.* 64:1914-1917.

30. Wang YQ, Li CG, & Pielak GJ (2010) Effects of Proteins on Protein Diffusion. *J. Am. Chem. Soc.* 132(27):9392-9397.

31. Hwang TL, Mori S, Shaka AJ, & vanZijl PCM (1997) Application of phase-modulated CLEAN chemical EXchange spectroscopy (CLEANEX-PM) to detect water-protein proton exchange and intermolecular NOEs. *J. Am. Chem. Soc.* 119(26):6203-6204.

32. Laemmli UK (1970) Cleavage of Structural Proteins During Assembly of Head of Bacteriophage-T4. *Nature* 227(5259):680-&.

33. Dolinsky TJ, Nielsen JE, McCammon JA, & Baker NA (2004) PDB2PQR: an automated pipeline for the setup of Poisson-Boltzmann electrostatics calculations. *Nucleic Acids Res.* 32:W665-W667.

34. Dolinsky TJ*, et al.* (2007) PDB2PQR: expanding and upgrading automated preparation of biomolecular structures for molecular simulations. *Nucleic Acids Res.* 35:W522-W525.

35. Baker NA, Sept D, Joseph S, Holst MJ, & McCammon JA (2001) Electrostatics of nanosystems: Application to microtubules and the ribosome. *Proc. Natl. Acad. Sci. U. S. A.* 98(18):10037-10041.

36. Ernst RR, Bodenhausen G, & Wokaun A (1990) *Principles of nuclear magnetic resonance in one and two dimensions* (Oxford University Press, New York, NY).

37. Wishart DS, Bigam CG, Holm A, Hodges RS, & Sykes BD (1995) ^{1}H, ^{13}C and 15N random coil NMR chemical shifts of the common amino acids. I. Investigations of nearest-neighbor effects. *J. Biomol. NMR* 5:67-81.

38. Wu D, Chen A, & Johnson C (1995) An Improved Diffusion-Ordered Spectroscopy Experiment Incorporating Bipolar-Gradient Pulses. *J. Magn. Reson.* 115:260-264.

Supplementary Tables

Supplementary Table 1. Experimental and estimated rotational correlation times and ^{15}N linewidths. Compilation of experimental rotational correlation times derived from DOSY and equation (3), together with computationally estimated and experimentally observed ^{15}N linewidths of SH3 upon addition of the DnaK chaperone.

	Experimental rotational correlation time (ns)	Estimated ^{15}N linewidth at half-height (Hz)	Experimental ^{15}N linewidth at half-height[1] (Hz)
Native SH3[2]	3.3	1.9	8.7
Unfolded SH3[2]	6.3	3.1[3]	8.9
DnaK[4]	124	54	N.A.

(1) averaged over all resonances.

(2) in NMR buffer, in the absence of DnaK.

(3) This estimate does not take into account the contribution of the viscosity imparted by the presence of SH3 in solution. In addition, this calculation assumes a rigid spherical body, to set an upper limit to the possible values that unfolded SH3 could attain. See Supplementary Table 2 and the accompanying discussion for additional considerations regarding the effect of viscosity, local motions and chemical exchange.

(4) or DnaK-protein complex, assuming a rigidly bound species tumbling approximately at the same rate as DnaK.

Supplementary Table 2. Computationally predicted ^{15}N NMR linewidths. Computationally predicted ^{15}N NMR linewidths of SH3 using viscosity of the buffer and of the solution in the presence of DnaK, respectively.

	Computed ^{15}N NMR linewidth in buffer (Hz)	Computed ^{15}N NMR linewidth in the presence of DnaK (Hz)
Native SH3	1.9	2.6
Unfolded SH3	3.1	4.6

Supplementary Table 3. Triple resonance NMR parameters

Experiment	Number of complex points (t1 x t2 x t3), t1: ^{13}C; t2: ^{15}N; t3: ^{1}H.	Sweep Widths (Hz)		
		^{1}H	**^{13}C**	**^{15}N**
3D CBCA(CO)NH	60 x 48 x 641	10000	10100	1935
3D HNCACB	96 x 48 x 641	10000	10100	1935
3D (HCA)CO(CA)NH	56 x 45 x 512	10000	1600	1905
3D HNCO	48 x 48 x 641	10000	1967	1935

Supplementary Figure Legends

Supplementary Figure 1. Proton chemical shift changes of SH3 upon addition of DnaK. (a)^{1}H,^{15}N HSQC amide proton chemical shift changes of native SH3 upon addition of a 4-fold excess of DnaK chaperone. (b) ^{1}H,^{15}N HSQC amide proton chemical shift resonance changes for unfolded SH3 upon addition of a 4-fold excess of DnaK chaperone. Missing bars denote residues whose intensities and volumes could not be accurately assessed due to resonance overlapping.

Supplementary Figure 2. Secondary chemical shifts of carbonyl NMR resonances in the presence and absence of DnaK. (a) Secondary chemical shifts of backbone carbonyl carbons (C') of (top) native SH3 and (bottom) native SH3 in the presence of 4-fold excess ADP-DnaK. (b) Secondary chemical shifts of backbone carbonyl carbons (C') of (top) unfolded SH3, and (bottom) unfolded SH3 in the presence of a 4-fold excess DnaK. The reported values were assessed by subtracting reference random coil shifts (37) from the measured chemical shifts.

Supplementary Figure 3. Mass spectrometry analysis of native gel bands. (a) Top: Mass spectrum for peptides eluted at 15.99 min in the native gel band sample. Bottom: Mass spectrum for peptides eluted at 16.07 min in liquid drkN SH3 sample. (b) Top: Mass spectrum for peptides eluted at 15.78 min in the native gel band sample. Bottom: Mass spectrum for peptides eluted at 14.32 min in liquid drkN SH3 sample.

Supplementary Figure 4.^{15}N NMR linewidth changes in the presence of DnaK. (a) Percent change in ^{15}N resonance linewidth-at-half-height of ^{1}H,^{15}N HSQC data for native SH3 upon addition of a 4-fold excess of DnaK chaperone. The observed average increases in linewidth are similar to the values expected for changes in viscosity due to the addition of DnaK (with no

binding taking place, see dashed line), as discussed on pages 4-5 of the SI Appendix. (b) Percent change in ^{15}N resonance linewidth-at-half-height of ^{1}H,^{15}N HSQC data for unfolded SH3 upon addition of a 4-fold excess of DnaK chaperone. Expected linewidth changes due solely to viscosity changes due to the addition of DnaK (with no binding taking place) are shown as a dashed line. (c) Percent change in ^{15}N resonance linewidth-at-half-height of ^{1}H,^{15}N HSQC data upon addition of a 4-fold excess of ADP-DnaK for new resonances in Figure 5 relative to the corresponding resonance of the unfolded state of SH3 in the absence of ADP-DnaK. In the case of more than one new resonance, the value shown is the mean linewidth change. Only residues which show new resonances are shown. In all panels, the missing bars pertain to residues whose intensities and volumes could not be accurately assessed due to resonance overlapping.

Supplementary Figure 5. NMR resonance volumes for the native state of SH3 (HSQC and HSQC CLEANEX-PM experiments). (a) ^{1}H,^{15}NHSQC resonance volumes of native SH3 in the (top) absence and (bottom) presence of a 4-fold excess ADP-DnaK. (b) ^{1}H,^{15}N HSQC CLEANEX-PM resonance volumes for native SH3 in the (top) absence and (bottom) presence of a 4-fold excess ADP-DnaK. All volumes were normalized to 64 scans.

Supplementary Figure 6. NMR resonance volumes for the unfolded state of SH3 (HSQC and HSQC CLEANEX-PM experiments). (a) ^{1}H,^{15}NHSQC resonance volumes of unfolded SH3 in the (top) absence and (bottom) presence of a 4-fold excess ADP-DnaK. (b) ^{1}H,^{15}N HSQC CLEANEX-PM resonance intensities for unfolded SH3 in the (top) absence and (bottom) presence of a 4-fold excess ADP-DnaK. All volumes were normalized to 64 scans.

Supplementary Figure 7. ^{1}H and ^{15}N backbone resonance assignments of native and unfolded SH3 in the presence of DnaK. Simulated ^{1}H,^{15}N HSQC NMR spectrum of SH3 in the presence of a 4-fold excess ADP-DnaK, showing backbone resonance assignments for the

folded (bold black) and unfolded (red with a prime ' character) species. Unlabeled red ellipses represent new resonances that appear only upon addition of DnaK.

Supplementary Figure 8. NMR pulse sequences used in Diffusion Ordered Spectroscopy (DOSY) experiments. a) The convection-compensated (cc) DOSY element (24) was inserted in front of the ^{1}H-^{13}C HSQC sequence, to compensate for the intrinsic convection in the NMR sample tube as well as to avoid proton exchange effect between water and amide in case ^{1}H-^{15}N HSQC is used instead of ^{1}H-^{13}C HSQC. Chemical shift evolution in the indirect dimension (t1) was acquired in the constant time mode (T=27ms). The δ, τ, ε and Δ values are set to 2ms, 4ms, 1.6ms and 100ms, respectively. The gradients are varied according to the one-shot scheme (25) to maintain the lock power and compensate for the imperfect 180° pulses during the bipolar-gradient pulses (38). sp1: hyperbolic secant pulse to excite aliphatic ^{13}C; sp2: square pulse to minimize excitation of CO; sp3: sinc pulse to excite the CO region only. The phase cycle is ϕ_1 = 8(x), 8(-x); ϕ_2 = 16(x), 16(-x); ϕ_3 = x, -x; ϕ_4 = x, x, y, y, -x, -x,-y -y; ϕ_{rec} = 2(x, -x, -x, x), 4(-x, x, x, -x), 2(x, -x, -x, x); ϕ_5 = 145°; ϕ_6 = 325°; ϕ_7 = 55°; ϕ_8 = 325°. Quadrature detection in the t1 dimension was achieved in Rance-Kay mode by altering the sign of ϕ_5 and G9. ϕ_3 and ϕ_{rec} phases change sign every other increment to remove axial peaks. The thin and thick lines represent 90° and 180° pulses, respectively. b) For natural abundance samples, the cc DOSY element was attached to the 3-9-19 WATERGATE sequence. The phase cycle is ϕ_1 = x, -x; ϕ_2 = 2(x), 2(-x); ϕ_3 = 4(x), 4(-x); ϕ_{rec} = x, -x, -x, x, -x, x, x, -x. In both pulse sequences, gradients G1… G9 have durations of 1.0, 1.0, 1.0, 0.5, 0.5, 1.0, 2.0, 0.5, 0.5 ms and powers of G_0× (1.0 - kappa), - G_0× (1.0 + kappa), 2.0 × kappa × G_0, ±36.1, 3.2, -38.1, 32.5, 5.4, 32.7 G/cm, respectively, with kappa set to 0.2 and G_0 varied among 5.4, 10.8, 21.7, 32.5 and 43.3 G/cm. WURST decoupling was employed in both sequences.

Supplementary Figure 9. Diffusion-Ordered Spectroscopy Data. a) Intensity decay curves documenting the DOSY experiments presented in this work via convection-compensated DOSY-HC-HSQC (24, 25). The y axis shows intensity differences relative to the HDO DOSY decays. (b) Viscosity-uncorrected and viscosity-corrected translational diffusion coefficients of native and unfolded SH3 in the absence and presence of a 4 fold excess of ADP-DnaK.

Supplementary Figures

Figure S1

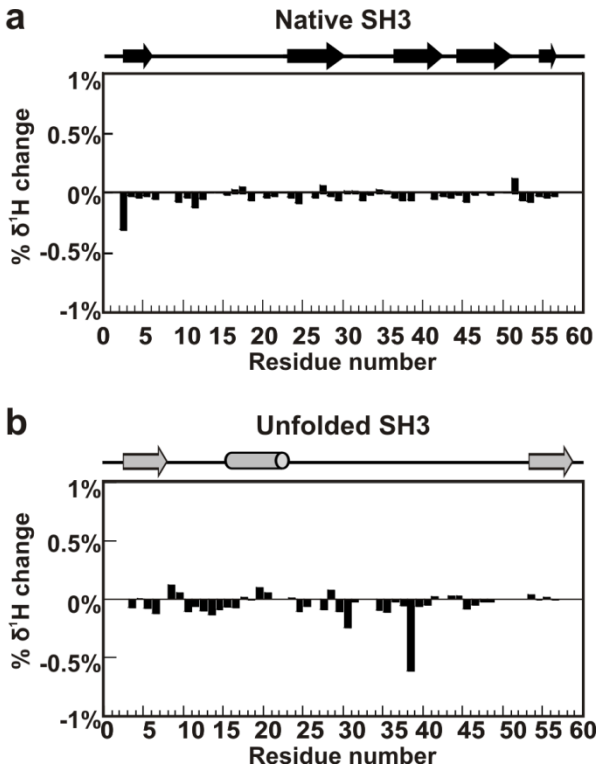

Figure S2

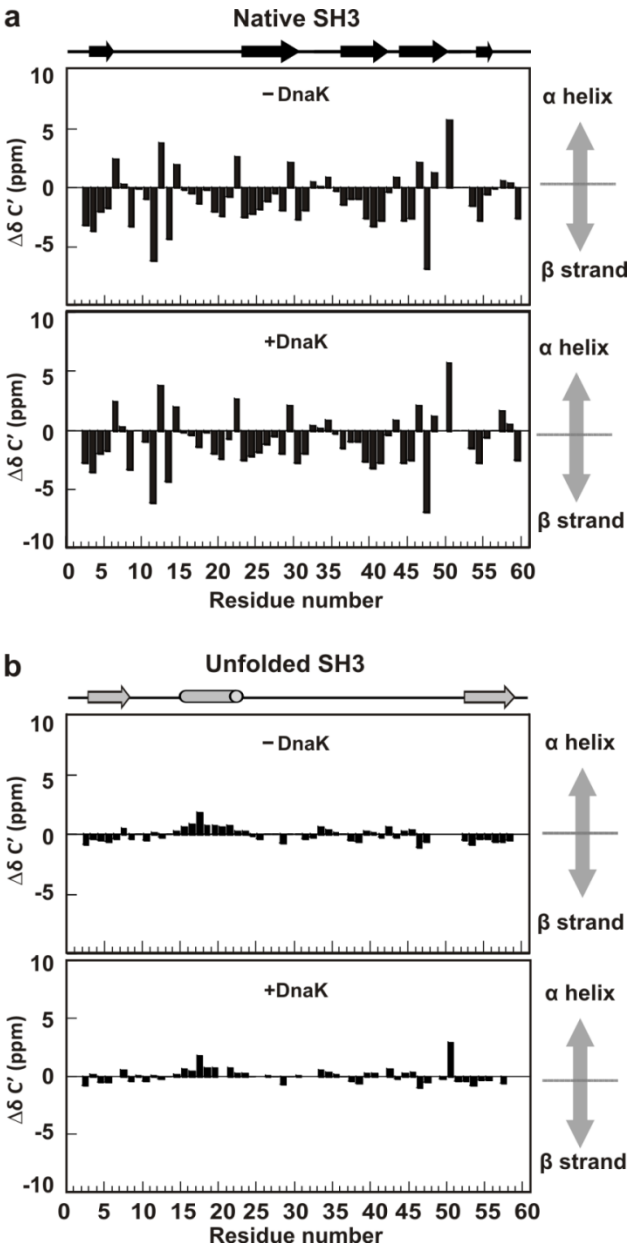
a
Native SH3
−DnaK
+DnaK
α helix
β strand
Δδ C′ (ppm)
Residue number
b
Unfolded SH3
−DnaK
+DnaK
α helix
β strand
Δδ C′ (ppm)
Residue number

Figure S3

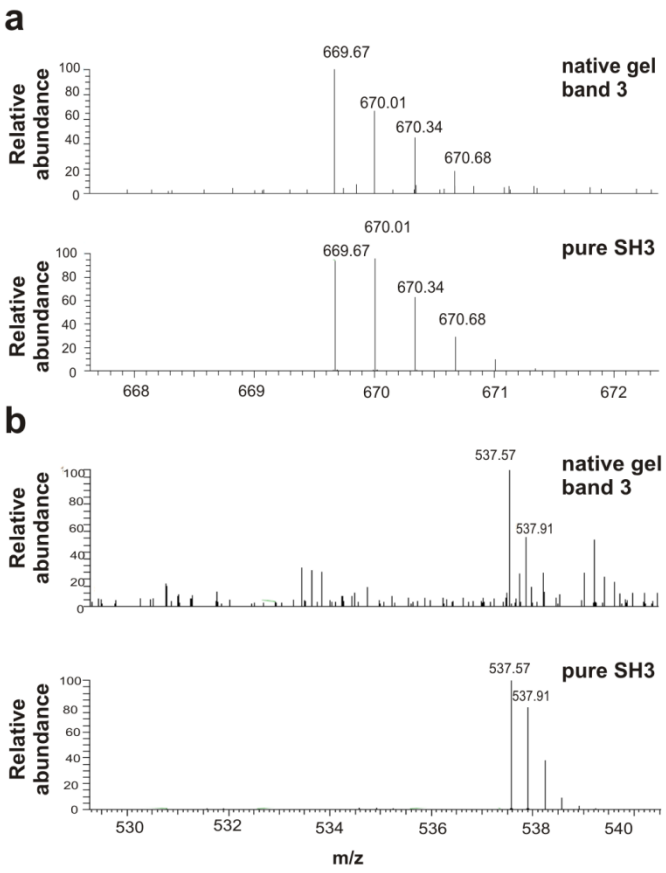
a
669.67
native gel band 3
670.01
670.34
670.68
Relative abundance
670.01
669.67
pure SH3
670.34
670.68
668
669
670
671
672
b
537.57
native gel band 3
537.91
537.57
pure SH3
537.91
530
532
534
536
538
540
m/z

Figure S4

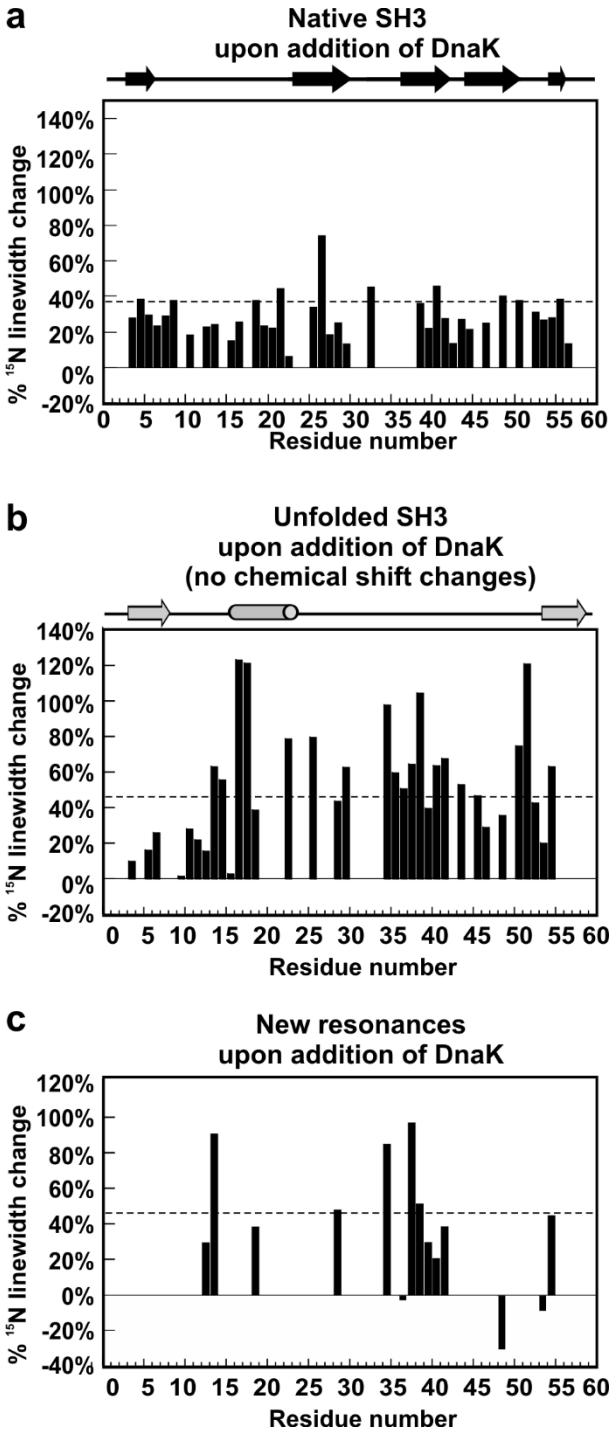
a
Native SH3
upon addition of DnaK
% 15N linewidth change
140%
120%
100%
80%
60%
40%
20%
0%
-20%
0 5 10 15 20 25 30 35 40 45 50 55 60
Residue number
b
Unfolded SH3
upon addition of DnaK
(no chemical shift changes)
% 15N linewidth change
140%
120%
100%
80%
60%
40%
20%
0%
-20%
0 5 10 15 20 25 30 35 40 45 50 55 60
Residue number
c
New resonances
upon addition of DnaK
% 15N linewidth change
120%
100%
80%
60%
40%
20%
0%
-20%
-40%
0 5 10 15 20 25 30 35 40 45 50 55 60
Residue number

Figure S5

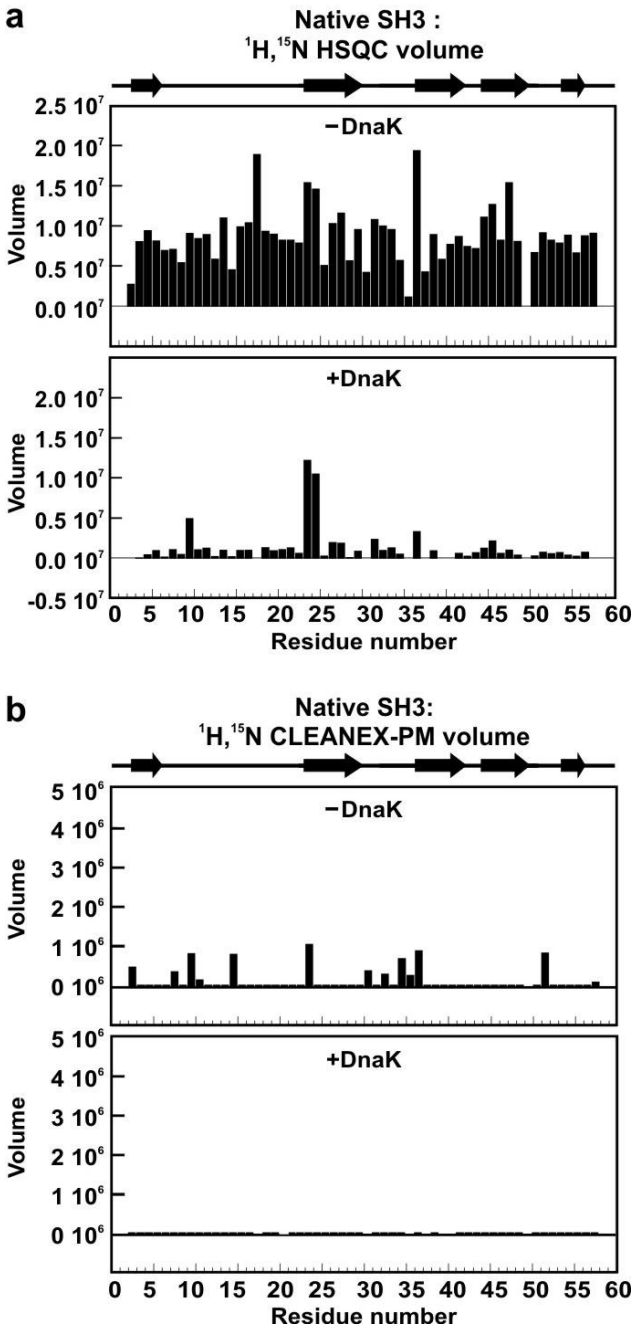
a
Native SH3 :
$^{1}H,^{15}N$ HSQC volume
−DnaK
+DnaK
Volume
2.5 10^7
2.0 10^7
1.5 10^7
1.0 10^7
0.5 10^7
0.0 10^7
-0.5 10^7
0 5 10 15 20 25 30 35 40 45 50 55 60
Residue number
b
Native SH3:
$^{1}H,^{15}N$ CLEANEX-PM volume
−DnaK
+DnaK
Volume
5 10^6
4 10^6
3 10^6
2 10^6
1 10^6
0 10^6
0 5 10 15 20 25 30 35 40 45 50 55 60
Residue number

Figure S6

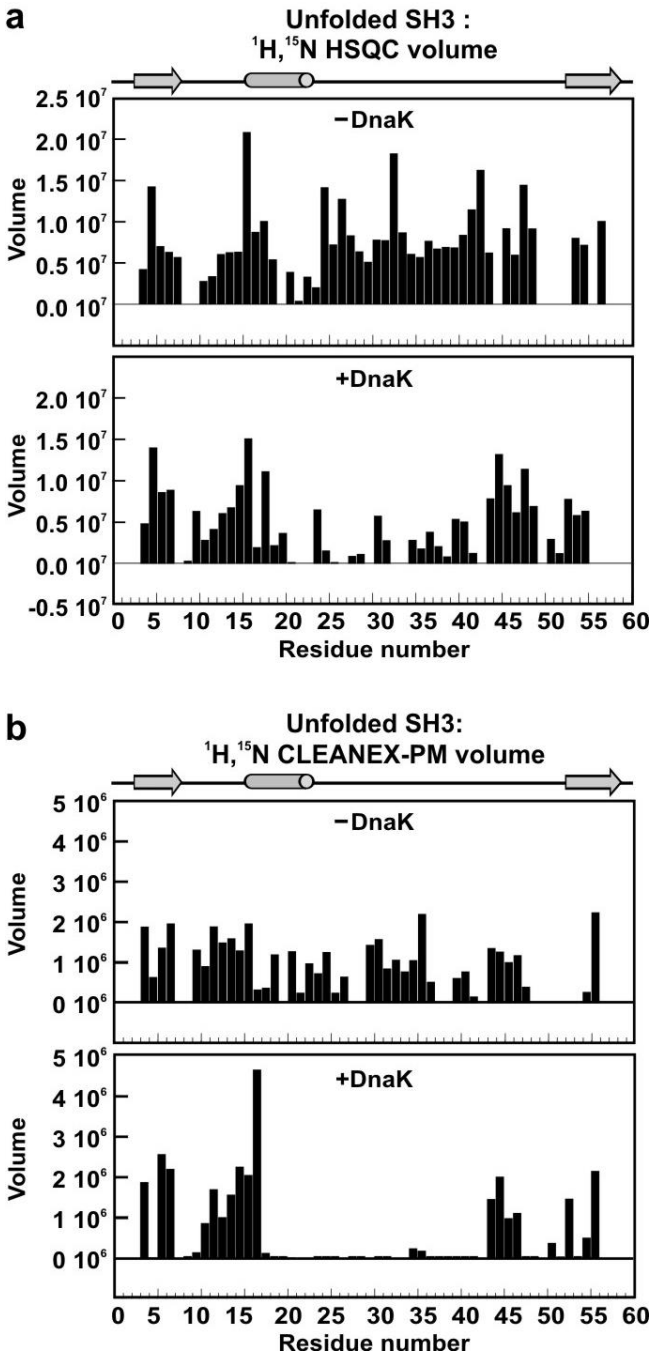
a
Unfolded SH3 :
$^{1}H,^{15}N$ HSQC volume
−DnaK
+DnaK
Volume
2.5 10^7
2.0 10^7
1.5 10^7
1.0 10^7
0.5 10^7
0.0 10^7
-0.5 10^7
0 5 10 15 20 25 30 35 40 45 50 55 60
Residue number
b
Unfolded SH3:
$^{1}H,^{15}N$ CLEANEX-PM volume
−DnaK
+DnaK
Volume
5 10^6
4 10^6
3 10^6
2 10^6
1 10^6
0 10^6
0 5 10 15 20 25 30 35 40 45 50 55 60
Residue number

Figure S7

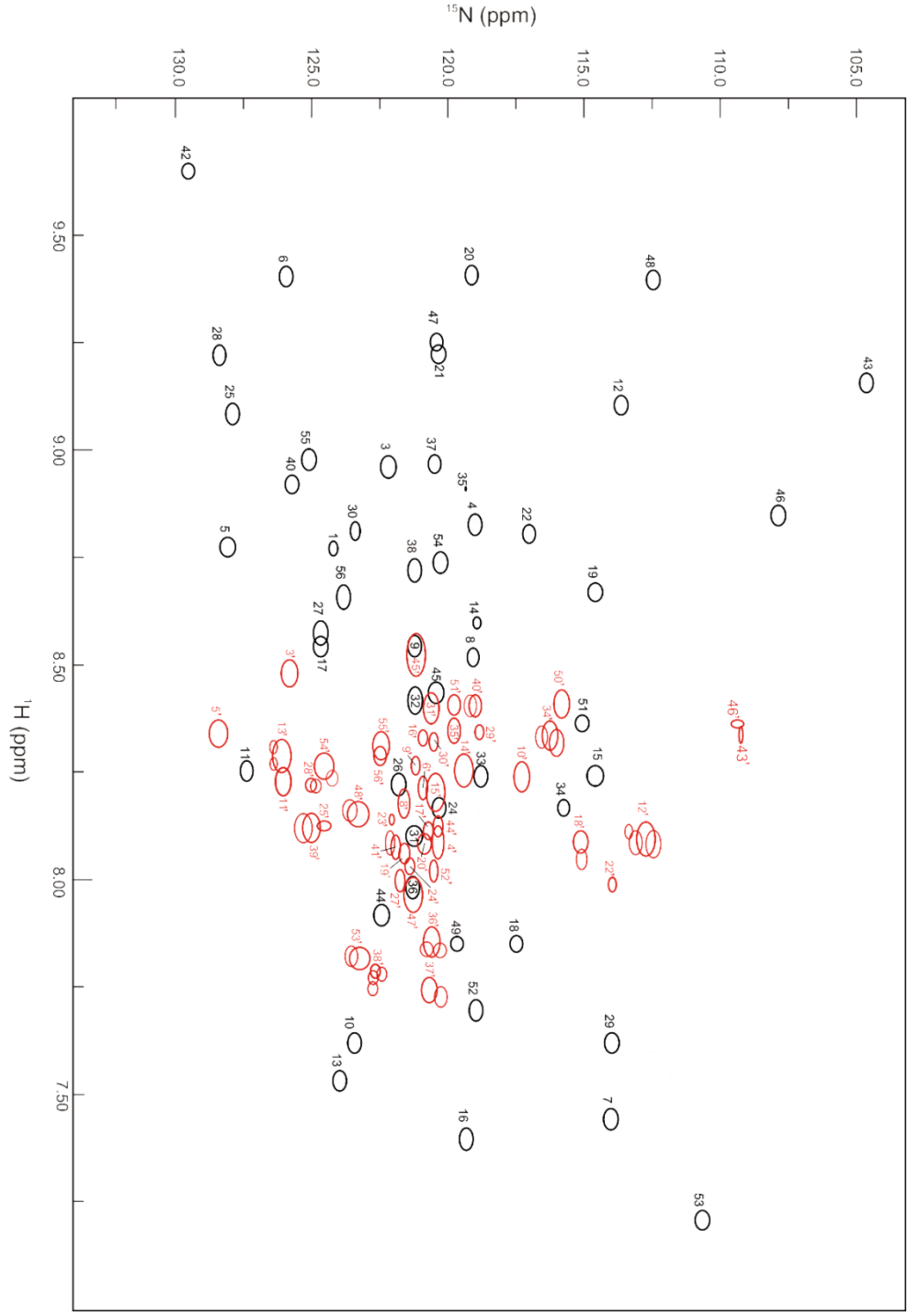
^{15}N (ppm)
105.0
110.0
115.0
120.0
125.0
130.0
^{1}H (ppm)
9.50
9.00
8.50
8.00
7.50

Figure S8

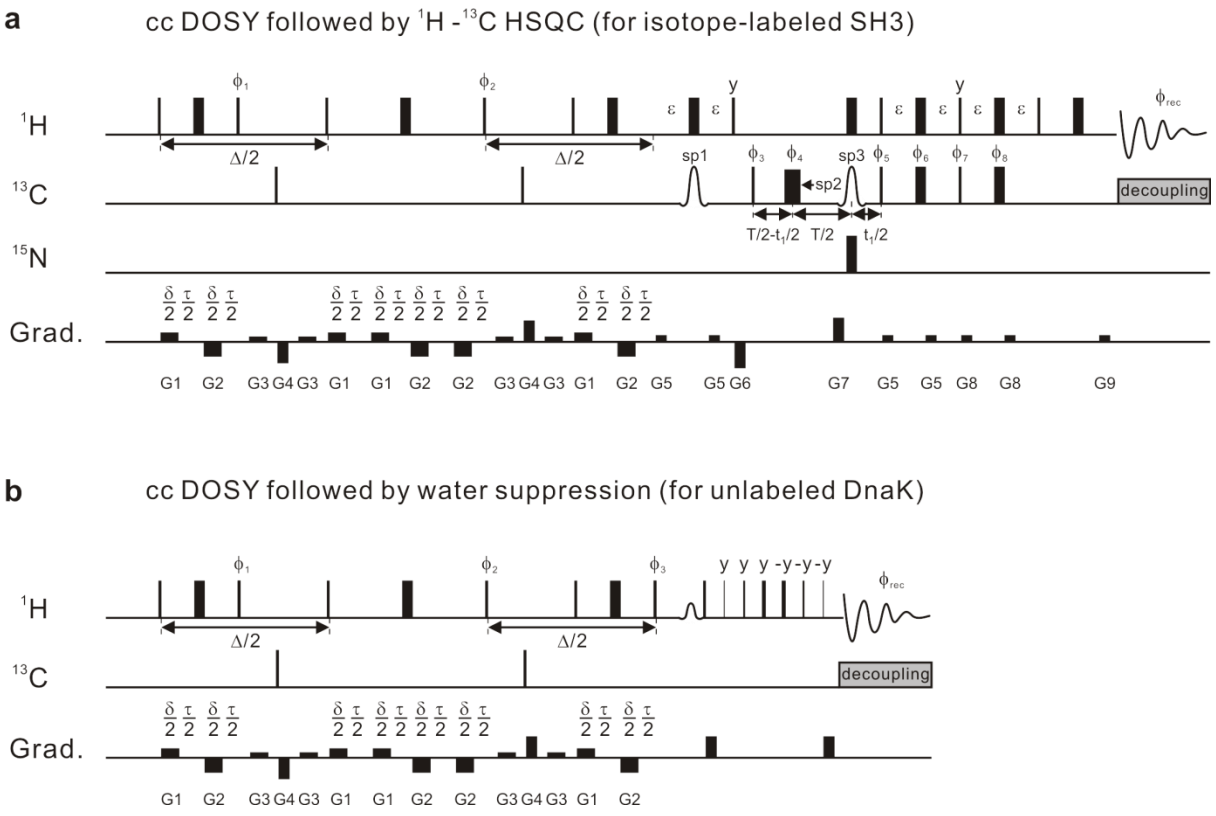
a
cc DOSY followed by ^{1}H -^{13}C HSQC (for isotope-labeled SH3)
^{1}H
^{13}C
^{15}N
Grad.
Δ/2
sp1
sp2
sp3
decoupling
T/2-t$_1$/2
T/2
t$_1$/2
G1 G2 G3 G4 G3 G1 G1 G2 G2 G3 G4 G3 G1 G2 G5 G5 G6 G7 G5 G5 G8 G8 G9
b
cc DOSY followed by water suppression (for unlabeled DnaK)
^{1}H
^{13}C
Grad.
Δ/2
decoupling
G1 G2 G3 G4 G3 G1 G1 G2 G2 G3 G4 G3 G1 G2

Figure S9

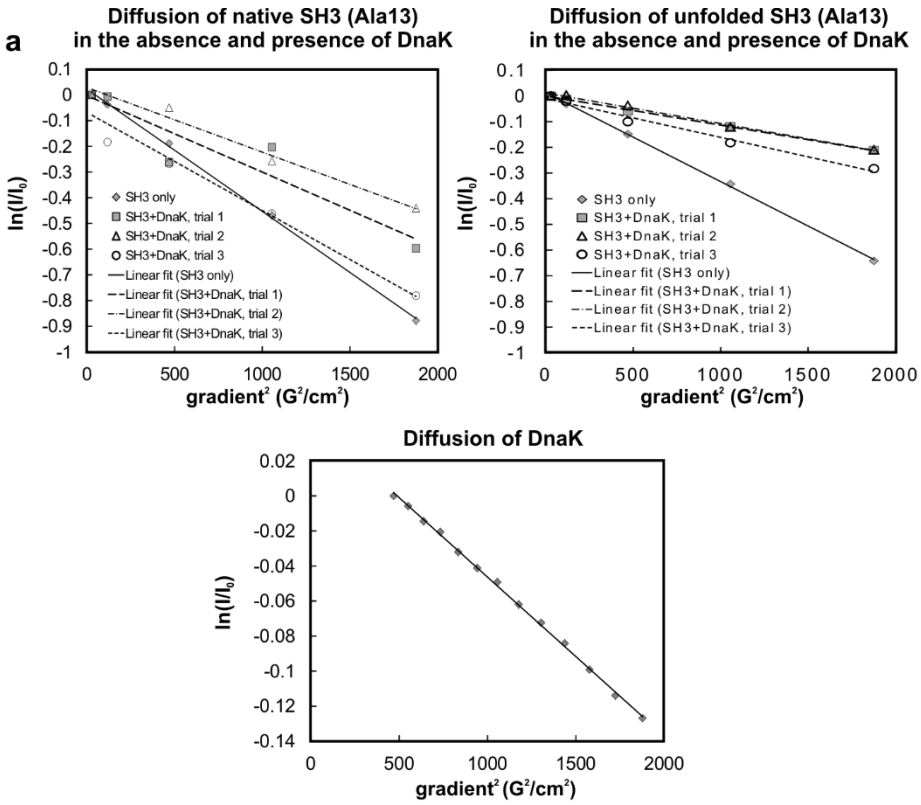
a
Diffusion of native SH3 (Ala13) in the absence and presence of DnaK
Diffusion of unfolded SH3 (Ala13) in the absence and presence of DnaK
ln(I/I0)
gradient² (G²/cm²)
SH3 only
SH3+DnaK, trial 1
SH3+DnaK, trial 2
SH3+DnaK, trial 3
Linear fit (SH3 only)
Linear fit (SH3+DnaK, trial 1)
Linear fit (SH3+DnaK, trial 2)
Linear fit (SH3+DnaK, trial 3)
Diffusion of DnaK

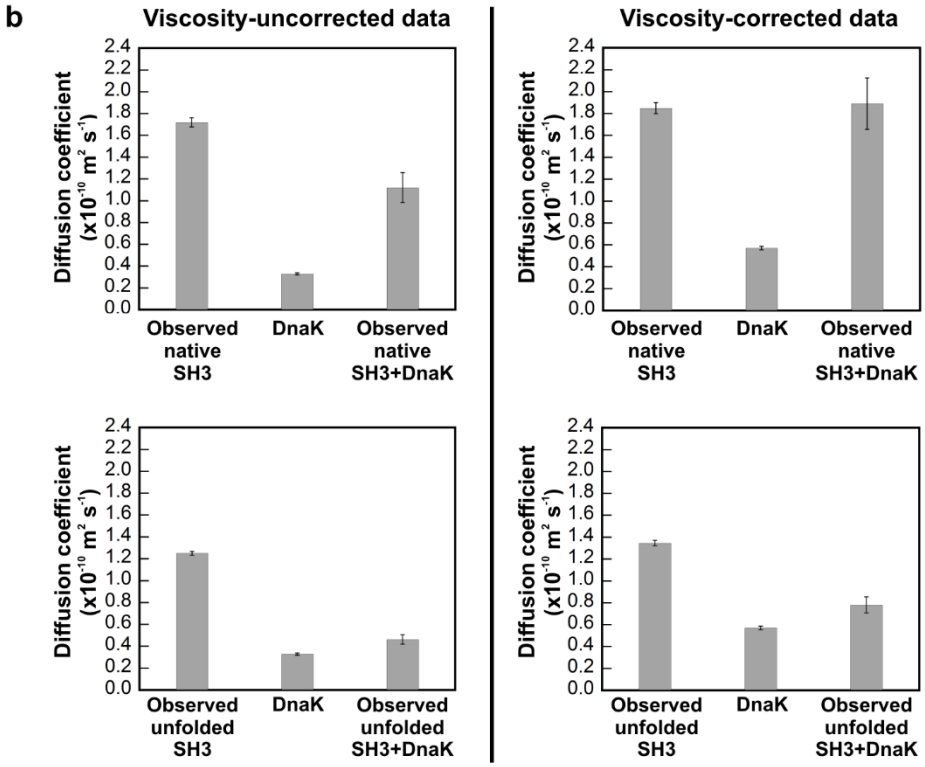
b
Viscosity-uncorrected data
Viscosity-corrected data
Diffusion coefficient (x10⁻¹⁰ m² s⁻¹)
Observed native SH3
DnaK
Observed native SH3+DnaK
Observed unfolded SH3
Observed unfolded SH3+DnaK